Research Square

Preprints are preliminary reports that have not undergone peer review.
They should not be considered conclusive, used to inform clinical practice,
or referenced by the media as validated information.

High Sensitivity Hemoglobin Biosensing Using a Plus Shaped Gold Metasurface Refractive Index Sensor

Syed Musthafa

sdmustafa88@gmail.com

Mohamed Sathak Engineering College

Faizal Mukthar Hussain

Jaya engineering college

Ahamed Hussain Asif

Mohamed Sathak Engineering College

AmanullaKhan Mahaboob Khan

Mohamed Sathak Engineering College

Research Article

Keywords:

Posted Date: October 23rd, 2026

DOI: https://doi.org/10.21203/rs.3.rs-11174650/v1

License: This work is licensed under a Creative Commons Attribution 4.0 International License.
Read Full License

Additional Declarations: No competing interests reported.

HIGH SENSITIVITY HEMOGLOBIN BIOSENSING USING A PLUS SHAPED GOLD METASURFACE REFRACTIVE INDEX SENSOR

Syed Musthafa Gani Shaik Fareed[1*] Faizal Mukthar Hussain Syed Moomin[2] Ahamed Hussain Asif Noorul Nawas[3] AmanullaKhan Mahaboob Khan[4]

[1,3] Department of Electrical and Electronics Engineering, Mohamed Sathak Engineering College,Kilakarai.Tamilnadu,India.
[2]Department of Computer Science and Engineering, Jaya Engineering College,Chennai.Tamilnadu,India
[4]Department of Electronics and Communication Engineering, Mohamed Sathak Engineering College,Kilakarai. Tamilnadu,India

[1] http://orcid.org/0000-0001-6352-0933, [2]http://orcid.org/ 0000-0001-9369-327X, [3]http://orcid.org/0009-0002-0102-9748 ,[4]http://orcid.org/0000-0002-5227-5693

Email: * sdmustafa88@gmail.com, faizaldwyc@gmail.com asifnawas02@gmail.com, amanulla82@gmail.com

ARTICLE INFO

Article History
Received: Month 01th, 20XX
Accepted: Month 15th, 20XX
Published: Month 30th, 20XX

Keywords:
Bio sensor
Hemoglobin
Metasurface
GST
Tunablity
Refractive Index

ABSTRACT

Hemoglobin concentration is one of the most important clinical parameters for diagnosis of anemias or cardiovascular diseases but label-free accurate quantification of this is still reliant on bulky laboratory infrastructure. A gold with Germanium Antimony Tellurium ($Ge_2Sb_2Te_5$) metasurface is called GST with a Plus shape is proposed here as a reconfigurable intelligent surface for hemoglobin detection. Localized surface plasmon resonance oscillations of the gold resonators are analyzed to establish the unit cell geometry and optical properties of hemoglobin within its physiological refractive index range to specify the sensing window. Gold is chosen for its chemical stability and plasmonic strong confinement of the plasmonic field, in the RIS configuration a reconfigurable layer is added to retune the resonant behavior after fabrication. Using numerical simulation, the absorption, electric-field, and magnetic-field response is evaluated, and the response to the geometric changes is analyzed. The spectral response is obtained and key geometrical parameters are optimized systematically to maximize the sensitivity. The design is then compared to reported hemoglobin sensors using metasurfaces. The maximum sensitivity of the crystalline GST is 766.67 nm/RIU which exceeds the maximum sensitivity of amorphous GST, 700 nm/RIU. The thickness of the substrate is 0.6 micrometers and metasurface is 0.3 micrometers. The crystalline GST is more sensitive than the amorphous GST. Then the suggested sensor is compared in contrast to the previous designed ones that are already published. The comparison shows that the designed design is able to identify the smaller change compared to the alternatives, thus it could be proposed as the basis to be developed further for medical sensors.

Copyright ©2025 by authors and Galileo Institute of Technology and Education of the Amazon (ITEGAM). This work is licensed under the Creative Commons Attribution International License (CC BY 4.0).

I. INTRODUCTION

The appearance of sugar, urine and hemoglobin can give an early warning of disease. With so many more patients having these conditions now, it has become more important to catch these diseases earlier. Plasmonic biosensors based on refractive index (RI) change are very sensitive, and can be used for challenging detection tasks. Biosensors combine biological elements with physical and chemical elements, and are able to detect biochemical substances. These include optical type, silicon-based type and magnetoelastic type.The advantage of optical biosensors, is that they are cheap, respond rapidly to nanoparticles, work fast and do not involve any invasive procedure. They tend to be divided into two categories; that is, labeled and label-free. There are two types of sensors: label-free and labeled. A label-free sensor interacts directly with a given analyst, while a labeled sensor is one that makes use of a tag that generates a detection signal. In contrast to a fully labeled system, a label-free biosensor is more specific, provides real-time measurement, is extremely sensitive and cheap. They are also easily and rapidly calculated. There are two types of commercial SPR sensors.

There are two basic configurations, Kretschmann and Otto. They all detect individual molecules by measuring effects on the sensor surface, based on the instructions given to the sensor. The approach is useful for electronic, biochemical and optical applications; and scientists have used it for medicine and environmental monitoring. SPR is frequently used in preference of biomolecule labelling for real time analysis: more easily observe complex structures; biomolecular recognition. The same configurations can be used on various types of biosensors. The use of nanocomposite layers can enhance the sensibility of biosensors in the course of maintaining low costs. In short, the newly-developed surface plasmon resonance (SPR) sensor made of Diamond Ring Fiber (DRF) can work well to detect biochemical and biological analytes

II. THEORETICAL REFERENCE

To diagnose disorders of the blood, it is important to measure hemoglobin accurately; that is, the sensing platform should be able to recognize a very slight alteration of the concentration of the protein, even in complex biological samples. Label-free, uneven samples are generally not presented well in traditional micro-optical cavities and interferometers, as the near field sensing region is not large enough for a reliable measurement [1]. To overcome these restrictions, the researchers explore metasurfaces with shapes resembling a plus sign (+) that are engineered to be made of gold. They serve as reconfigurable surfaces, capable of compressing all the incoming electromagnetic energy into resonance cavities of high intensities, boosting light–matter interaction, and providing more accurate analysis of the target molecules [2,3]. By altering the metasurface geometry, the electromagnetic response of the metasurface also changes and can be tuned to better respond to hemoglobin, to enhance detection sensitivity [4]. This approach provides a solution to the limitations of the traditional optical biosensing which is not always sensitive enough to that of the expensive and labor intensive labelling method [5].

Nanophotonic designs give more power to the interaction between light and matter; such designs can create high quality factor resonances capable of providing molecular signatures without labels [6] [7]. Their subwavelength structures cause the optical field to focus down into small volumes, thus enabling the detection of small amounts of biomolecules [8]. The sensing platform combines these functions without any spectrometer, thus eliminating the bulky and costly equipment typically used in a diagnostic test and allows high-throughput diagnostic tests [9], [10]. Active surfaces can also modify EM waves in space and in wavelength, solve the lack of target specificity of the passive designs and make nanophotonic sensors closer to the clinical world [11] [12]. For metals, the resonance is associated with the behaviour of a collective motion of conduction electrons. Near field can be enhanced and its spectral response can be manipulated by subwavelength plus-shaped resonators [13]. The so-called “hot spots” created by the localized surface plasmon resonances allow excellent confinement of incident electromagnetic energy down to deep-subwavelength dimensions, thereby enhancing light – matter interaction at the molecular scale [14]. Generally, reconfigurable surfaces also have to include active materials, including liquid crystals and electrostatic gates, that alter the refractive index of the surrounding material, such as to tune these resonances [15] [16]. It has been possible to rotate the local dielectric environment or to change the shape of the plus-shaped meta-atoms on the device, also altering the resonant frequency [17]. This results in a shift in hemoglobin concentration due to the change of the refractive index in the enhanced near field region as influenced by the dielectric properties of hemoglobin. A change in the plasmonic resonance condition induced by a change in the local refractive index when hemoglobin is loaded results in the measurable spectral response [19]. The shift of the resonance frequencies is visible by shifts in transmission or reflection spectra and can be used as a good indication of the hemoglobin concentration present in the sensing volume [20].

This is based on the high sensitivity of high-Q resonances to changes of the local state of the dielectric environment. It thus offers a quantitative means to monitor the refractive index changes of hemoglobin [21] The near-field refractive index increases and the resonance shifts to larger wavelengths as the hemoglobin concentration increases since the effective optical path is larger [22, 23]. The change in molecular binding has the effect of perturbed dielectric environment around the hotspot and hence the spectrum can be used to follow binding, in real time [24] [25]. They can also be incorporated into the metallic unit cells active devices, which can be adjusted during the dispersion and increase the detection of selected protein concentrations [26]. Tuning of the response will also allow the identification of weak absorption signatures; hemoglobin has been separated from other complex biomolecules in the sample [27]. Metasurface designs also overcome the drawbacks of static devices and are able to enable high-throughput point-of-care medical diagnostics [28]. The platform integrates plasmonic confinement with programmable spectral control and allows for label-free detection of molecule binding and delivers exquisite electronic transduction of binding events [29]. It can be helpful to subtract the structural resonance from the environmental background noise to separate the signal of interest from the background to provide an improved signal-to-noise ratio in a complex biological fluid [30].

III. DESIGN AND NUMERICAL MODELING OF A PLUS-SHAPED HEMOGLOBIN BIOSENSOR

A biosensor uses a gold metasurface whose refractive index can be tuned. This tunability comes from GST, which has two material states: amorphous and crystalline. Combining GST with the metasurface geometry also improves the refractive-index sensor’s sensitivity. The model is presented and assessed through its electric field, absorption, and magnetic-field responses. Several changes to the geometric parameters are examined as well. Varying the angle of incidence shows how the absorbed portion of the design changes.

The proposed model was compared with existing designs, and the results show a clear advantage in sensitivity. Its performance also suggests that the biosensor could be integrated into clinical sensing devices. Figure 1 presents the GST-based metasurface structure: a 0.3 μm gold metasurface sits on a 0.6 μm GST substrate, while a second gold layer forms the 0.3 μm ground plane. Biomolecules are placed on the upper gold surface. Figure 1(a) shows the three-dimensional front view; Figures 1(b) and 1(c) provide the top and two-dimensional views, respectively. GST in its crystalline phase produces higher sensitivity than the amorphous phase.

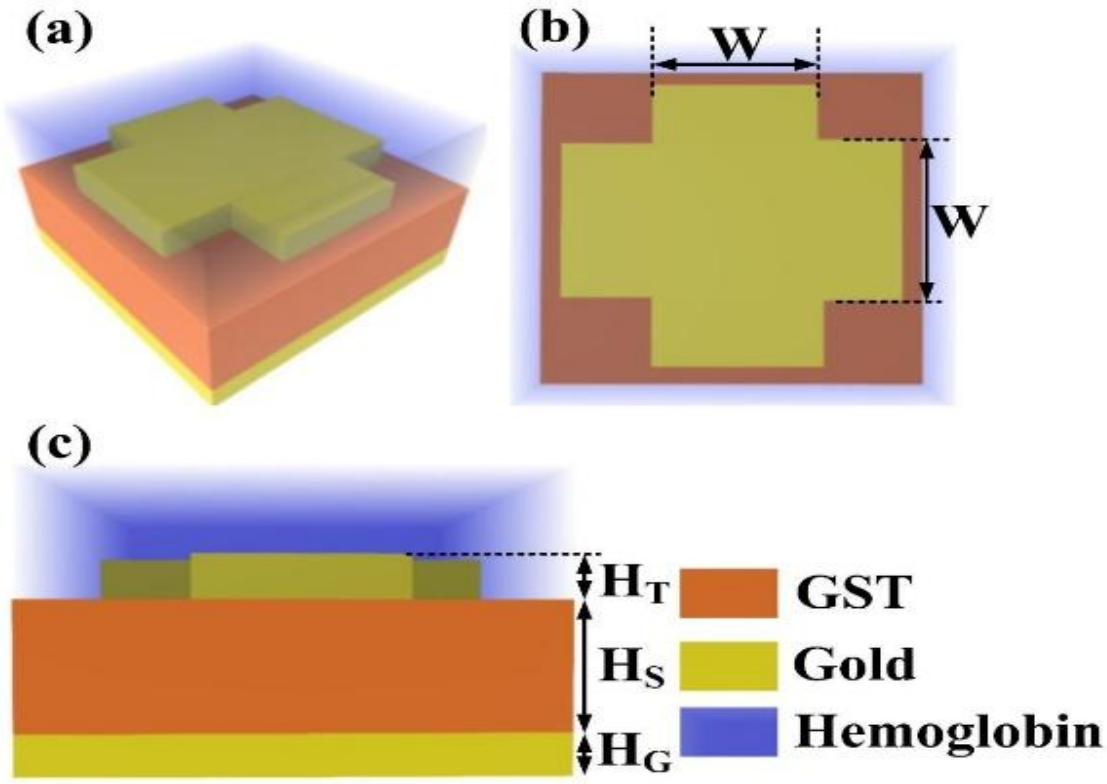

Figure 1: Plus Shaped GST based metasurface biosensor
(a)-Perspective View (b)-Overhead view (c)-Frontal view

III.1 ANALYSIS OF METASURFACE

Metasurface analysis is central to this design. Its effective permittivity and permeability can be obtained from the simulated reflection and transmission coefficients using Equations (1–5). Here, S_{11} denotes reflection coefficient, while S_{21} denotes transmission coefficient the simulated values are substituted into the equations to determine the metasurface parameters.

The Impedance (Z) is given by,

$$z = \pm\sqrt{\frac{(1+S_{11})^2 - S_{21}^2}{(1-S_{11})^2 - S_{21}^2}} \quad (1)$$

$$e^{ink_0d} = \frac{S_{21}}{1 - S_{11}\frac{z-1}{z+1}} \quad (2)$$

The refractive index can be calculated as,

$$n = \frac{1}{k_0 d}[\{[\ln e^{ink_0d}]'' + 2m\pi]\} - i[\ln(e^{ink_0d})]'] \quad (3)$$

The permitivity is ,

$$\varepsilon = \frac{n}{z} \quad (4)$$

The permeablity is,

$$\mu = n\, z \quad (5)$$

The sensitivity is calculated from wavelength peak difference for different refractive index biomolecules.

$$S = \frac{\Delta\lambda}{\Delta n} \quad (6)$$

$\Delta\lambda$ = Change in wavelength

Δn=Change in Refractive Index

IV. RESULTS AND DISCUSSIONS

IV.1 ABSORPTION ANALYSIS

The biosensor shown in Figure 1 was examined in COMSOL Multiphysics through the finite element method (FEM). Figures 2–5 present the resulting absorption and electric-field responses, along with changes produced by varying the angle and other geometric parameters. Absorption results for aGST and cGST are also provided in Figures 2–5. The design was evaluated at four hemoglobin concentrations, ranging from 10 g/l to 40 g/l in 10 g/l increments. The corresponding refractive indices were 1.34, 1.36, 1.39, and 1.43. Results were recorded for wavelengths between 0.6 µm and 1 µm.

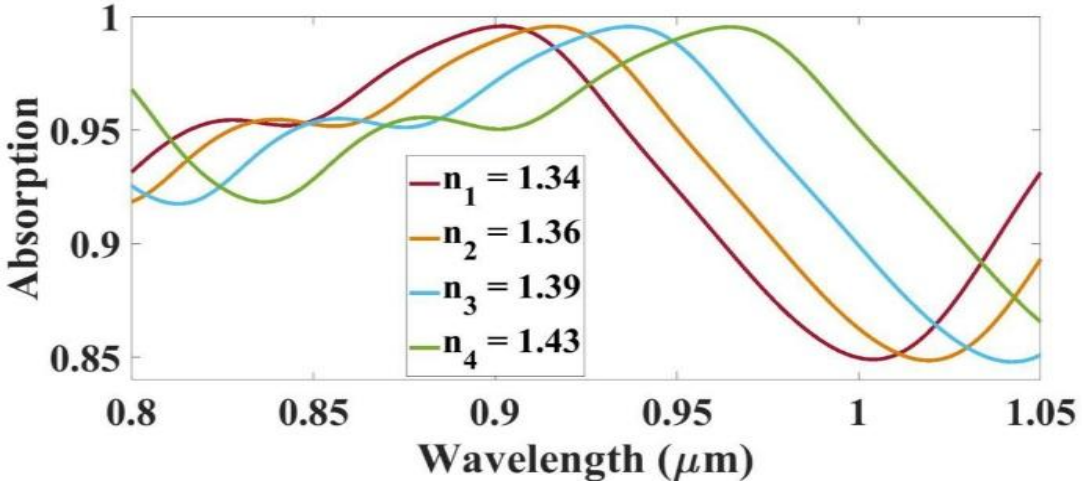

Figure 2 Effect of Concentration Variation on Absorption in the aGST Phase

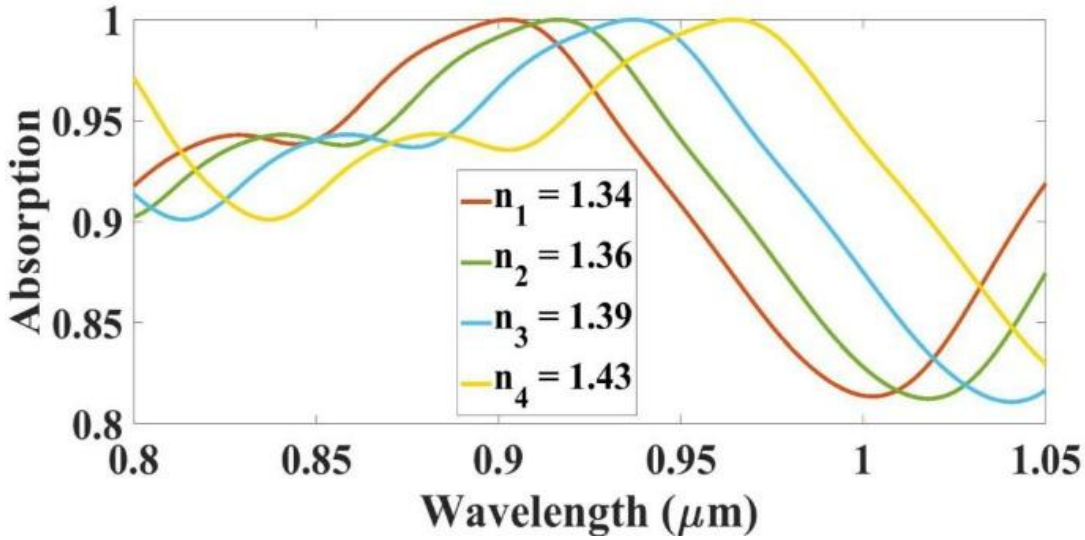

Figure 3 Effect of Concentration Variation on Absorption in the cGST Phase

Figure 2 shows the absorption of aGST at various concentrations, and it is understandable to observe how the wavelength peak differs between each of them. Peak wavelengths can be detected anywhere between 0.9 µm and 0.97µm when investigating different hemoglobin concentrations. In Figure 3 shows the absorption of wavelength of cGST at various concentrations, Peak wavelengths for various hemoglobin concentrations can be found anywhere between 0.902 µm and 0.968 µm. The peak wavelength of a cGST is 0.902 µm, while that of an aGST is 0.903 µm. These two types of GST material are responsible for the tunability of about 28 nm.

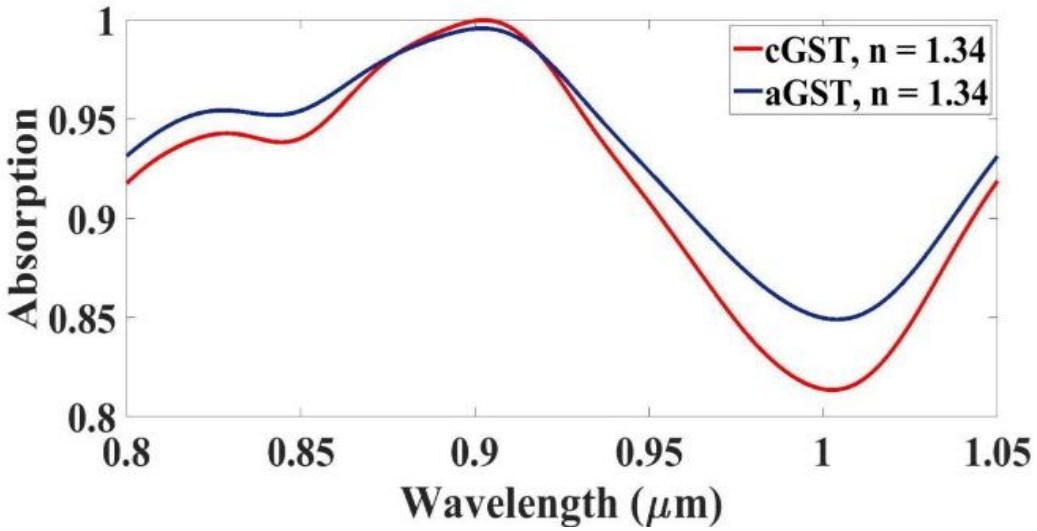

Figure 4 Effect of Concentration Variation on Absorption data for biomolecules with n=1.34

The Figure 4 compares aGST and cGST at a hemoglobin biomolecule concentration with a refractive index (RI) of 1.34.The cGST and aGST peaks occur at wavelengths of 0.902 μm and 0.903 μm, respectively. Switching between the two GST material modes produces a tunability range of 28 nm.

Table 1: Sensitivity Analysis of aGST and cGST material for various Refractive Indexes

Phase Change Materials	**Refractive Index Ranges from n=1.34 to n=1.43**	**n1**	**n2**	**n3**	**n4**
		1.34	1.36	1.39	1.43
	Change in Refractive Index Δn	0.02	0.03	0.04	
Amorphous phase of GST aGST	**λ (μm)**	0.902	0.916	0.937	0.965
	Change in wave length Δλ (μm)	0.014	0.021	0.028	
	Sensitivity S (nm/RIU)	700	700	700	
Crystalline phase of GST cGST	**λ (μm)**	0.903	0.918	0.941	0.968
	Change in wave length Δλ (μm)	0.015	0.023	0.027	
	Sensitivity S (nm/RIU)	750	**766.67**	675	

Table 1 compares the aGST and cGST values across the full range of hemoglobin concentrations. Sensitivity is calculated as the ratio of the RI difference to the wavelength difference, according to Equation (1). Both methods detect hemoglobin, with sensitivity values ranging from 675 nm/RIU to 766.67 nm/RIU

IV.2 VARIATION IN GEOMETRICAL PARAMETERS IN THE ABSORPTION OF HEMOGLOBIN

For the Plus Shaped GST metasurace design, various geometric factors such as the substrate thickness,Gold resonator thickness are changed in the numerical simulation and to analyze how the changes affect the absorption results, and the outcomes are given in Figures (5–8).

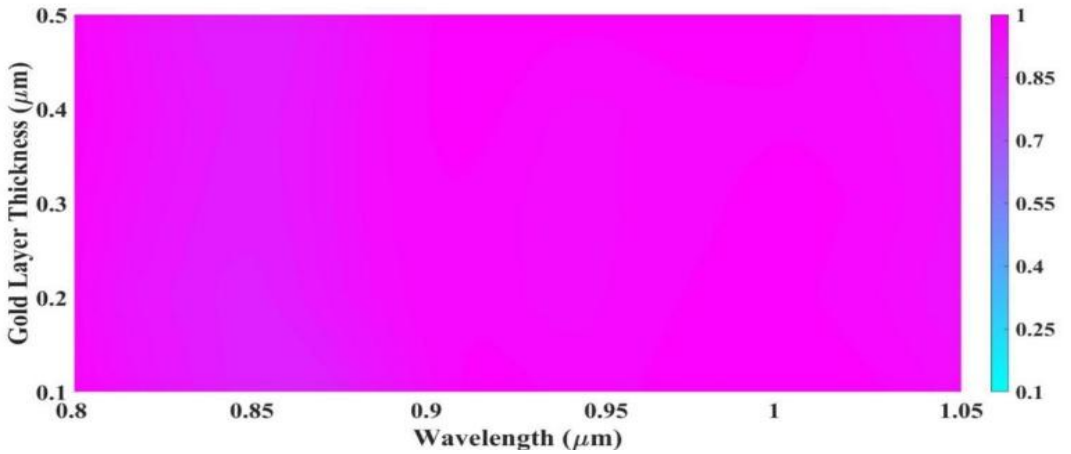

Figure 5 Variation in Gold Ground Layer Thickness on Hemoglobin Absorption

Figure 5 shows absorption values for ground-layer thicknesses between 0.1 and 0.5 micrometres. This layer matters because it prevents light transmission. The biosensor performs best at a thickness of 0.3 micrometres, where absorption reaches its highest value.

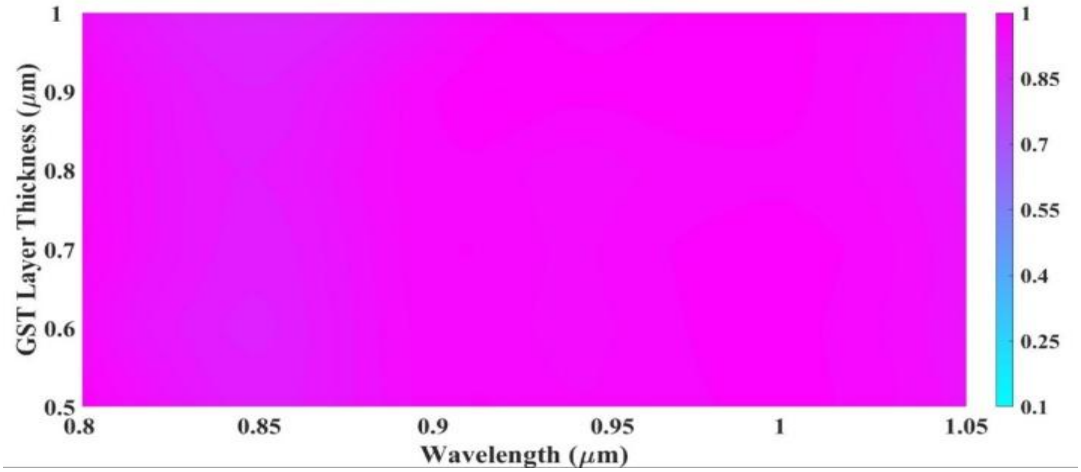

Figure 6 Variation in GST layer Thickness on Hemoglobin Absorption

Figure 6 shows the absorption values for substrates with densities ranging from 0.4 to 0.9 micrometers. Since the substrate absorbs most of the light striking the model, its density strongly affects performance. Absorption peaks at a substrate density of 0.6 micrometers, indicating that the biosensor model performs best at this value.

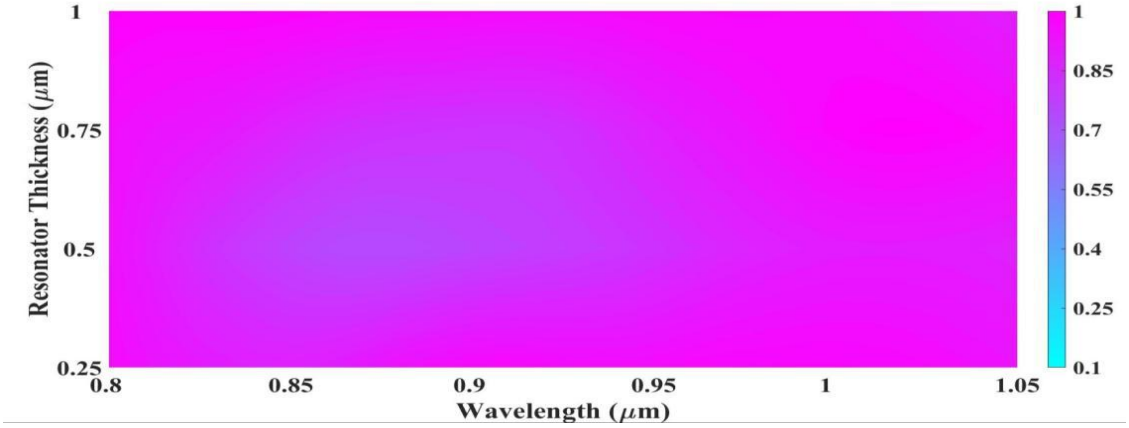

Figure 7 Variation in plus shape gold layer Thickness on Hemoglobin Absorption

Figure 7 shows how design choices, including resonator thickness, affect absorption during the aGST phase. The substrates range from 0.25 µm to 1 µm in thickness, with the biosensor reaching its highest absorption at a resonator thickness of 0.25 µm.

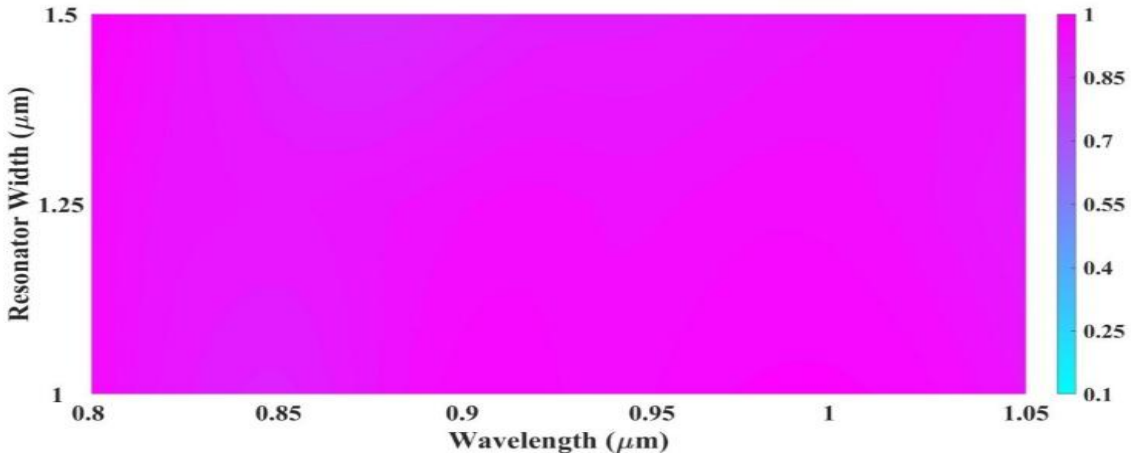

Figure 8 Variation in plus shape gold layer resonator width on Hemoglobin Absorption

Figure 8 shows the absorption values as the plus-shaped resonator width increases from 1 µm to 1.5 µm. Across this range, the width has little apparent effect on the absorption response at 1.25 µm.

IV.3 ANALYSIS OF ELECTRIC FIELD INTENSITY IN HEMOGLOBIN ABSORPTION

The results of the calculations for the electric field are shown in Figure 9 for three dissimilar wavelengths, specifically 0.85 µm, 0.902 µm, and 1 µm.

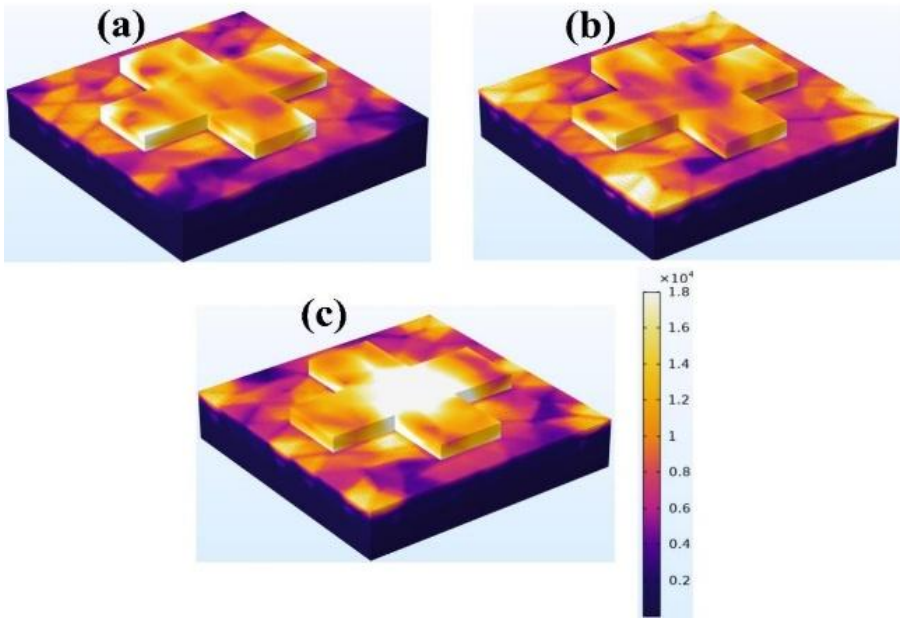

Figure 9 Variation in Electricfield of Plus shaped gold resonator metasurface biosensor for the wavelengths (a) 0.85 µm, (b) 0.902 µm, and (c) 1 µm

In the figure (a) indicates, the field is collected primarily at the arms and edges of the plus shaped resonator. It seems that the strongest areas are in the corners and metallic boundaries. The strong interaction between the incident electromagnetic wave and the plasmonic/metasurface is indicated by the appearance of these localized hot spots. Molecules or analytes which are close to these areas experience a significantly stronger field, resulting in a better refractive-index sensing.

In Fig. (b) the field pattern are located throughout the central plus-like shape and out through the substrate. The electromagnetic resonance can be modified by changes in the field pattern, indicating the changes in the sensing environment. The field enhancement is displayed in the figure c. A bright and intense area is sharply focused in the center of the plus-shaped resonator, with the intensity of the electric field close to the maximum displayed in the color scale.

As (a), (b), and (c) are different concentrations or refractive indices of the analytes, changes in the location and intensity of the hot-spots indicate the sensitivity of the metasurface to its surrounding medium. The figures clarify this pattern, and the electric-field analysis reaches the same conclusion. The strongest visible absorption occurs at a wavelength of about 0.902 μm.

V. CONCLUSIONS

This work presents a biosensor for detecting hemoglobin biomolecules. It combines a GST metasurface with a plus-shaped gold resonator, and its performance is evaluated through absorption responses across different hemoglobin concentrations. Sensitivity is calculated from the change in peak wavelength relative to the refractive index (RI). Crystalline GST reaches a maximum sensitivity of 766.67 nm/RIU, exceeding the 700 nm/RIU obtained with amorphous GST. The substrate is 0.6 μm thick, while the metasurface thickness is 0.3 μm. The gold ground-layer thickness and the width of the plus-shaped resonator are also varied to identify the best design parameters. Compared with previously published results, the proposed model performs better. It could therefore be used in clinical optical sensing applications.

Design	Sensitivity
Plus Shaped aGST based gold resonator based Biosenor [Proposed]	700 nm/RIU
Plus Shaped cGST based gold resonator based Biosenor [Proposed]	766.67 nm/RIU
[31]	65.7 nm/RIU
[32]	33 GHz/RIU
[33]	700 nm/RIU
[34]	294 nm/RIU
[35]	387 nm/RIU
[36]	1139 nm/RIU
[37]	500 nm/RIU
[38]	130 GHz/RIU

VI. AUTHOR'S CONTRIBUTION

Example:

Conceptualization: Syed Musthafa Gani Shaik Fareed[1]* Faizal Mukthar Hussain Syed Moomin[2] ,Ahamed Hussain Asif Noorul Nawas[3],AmanullaKhan Mahaboob Khan[4].
Methodology: Author One and Author Two, Author Three
Investigation: Author One and Author Two, Author Three
Discussion of results: Author One, Author Two and Author Three.
Writing – Original Draft: Author One.
Writing – Review and Editing: Author One and Author Two, Author Three
Resources: Author Two., Author Three
Supervision: Author Two and Author Three.
Approval of the final text: Author One, Author Two and Author Three.

VII. REFERENCES

[1] J. Qin *et al.* , "Metasurface Micro/Nano-Optical Sensors: Principles and Applications," *CityU Scholars* , vol. 16, no. 8, pp. 11598–11618, Aug. 2022, doi: 10.1021/acsnano.2c03310 .

[2] B. Liu, Y. Peng, Y. Hao, Y. Zhu, S. Chang, and S. Zhuang, "Ultra-wideband terahertz fingerprint enhancement sensing and inversion model supported by single-pixel reconfigurable graphene metasurface," *PhotoniX* , vol. 5, no. 1, Apr. 2024, doi: 10.1186/s43074-024-00129-4 .

[3] H. Kim, H. K. Yun, S. Jeong, S. Lee, E. Cho, and J. Rho, "Optical Metasurfaces for Biomedical Imaging and Sensing," *ACS Nano* , vol. 19, no. 3, pp. 3085–3114, Jan. 2025, doi: 10.1021/acsnano.4c14751 .

[4] J. Tian and W. Cao, "Reconfigurable flexible metasurfaces: from fundamentals towards biomedical applications," *PhotoniX* , vol. 5, no. 1, Jan. 2024, doi: 10.1186/s43074-023-00116-1 .

[5] A. V. Kabashin, V. G. Kravets, and A. N. Grigorenko, "Label-free optical biosensing: going beyond the limits," *Chemical Society Reviews* , vol. 52, no. 18, pp. 6554–6585, Jan. 2023, doi: 10.1039/d3cs00155e .

[6] N. Zhang *et al.* , "Deep-Learning Empowered Customized Chiral Metasurface for Calibration-Free Biosensing," *Advanced Materials* , vol. 37, no. 1, Oct. 2024, doi: 10.1002/adma.202411490 .

[7] M. Luo *et al.* , "High-Sensitivity Optical Sensors Empowered by Quasi-Bound States in the Continuum in a Hybrid Metal–Dielectric Metasurface," *ACS Nano* , vol. 18, no. 8, pp. 6477–6486, Feb. 2024, doi: 10.1021/acsnano.3c11994 .

[8] Z. Zhang *et al.* , "Advanced Terahertz Refractive Sensing And Fingerprint Recognition Through Metasurface-Excited Surface Waves," *Advanced Materials* , vol. 36, no. 14, Jan. 2024, doi: 10.1002/adma.202308453 .

[9] Y. Jahani *et al.* , "Imaging-based spectrometer-less optofluidic biosensors based on dielectric metasurfaces for detecting extracellular vesicles," *Nature Communications* , vol. 12, no. 1, p. 3246, May 2021, doi: 10.1038/s41467-021-23257-y .

[10] Y. Yang *et al.* , "Integrated metasurfaces for re-envisioning a near-future disruptive optical platform," *Light Science & Applications* , vol. 12, no. 1, p. 152, Jun. 2023, doi: 10.1038/s41377-023-01169-4 .

[11] T. Gu, H. J. Kim, C. Rivero-Baleine, and J. Hu, "Reconfigurable metasurfaces towards commercial success," *Nature Photonics* , vol. 17, no. 1, pp. 48–58, Dec. 2022, doi: 10.1038/s41566-022-01099-4 .

[12] B. I. Karawdeniya *et al.* , "Surface Functionalization and Texturing of Optical Metasurfaces for Sensing Applications," *Chemical Reviews* , vol. 122, no. 19, pp. 14990–15030, May 2022, doi: 10.1021/acs.chemrev.1c00990 .

[13] J. Hu *et al.* , "Rapid genetic screening with high quality factor metasurfaces," *Nature Communications* , vol. 14, no. 1, p. 4486, Jul. 2023, doi: 10.1038/s41467-023-39721-w .

[14] A. John-Herpin *et al.* , "Metasurface-Enhanced Infrared Spectroscopy: An Abundance of Materials and Functionalities," *Advanced Materials* , vol. 35, no. 34, May 2022, doi: 10.1002/adma.202110163 .

[15] C. Zeng *et al.* , "Graphene-empowered dynamic metasurfaces and metadevices," *Opto-Electronic Advances* , vol. 5, no. 4, p. 200098, Jan. 2022, doi: 10.29026/oea.2022.200098 .

[16] D.-H. Kang *et al.* , "Liquid crystal-integrated metasurfaces for an active photonic platform," *Opto-Electronic Advances* , vol. 7, no. 6, p. 230216, Jan. 2024, doi: 10.29026/oea.2024.230216 .

[17] Y. Ni, C. Chen, S. Wen, X. Xue, L. Sun, and Y. Yang, "Computational spectropolarimetry with a tunable liquid crystal metasurface," *eLight* , vol. 2, no. 1, Nov. 2022, doi: 10.1186/s43593-022-00032-0 .

[18] C. Huang *et al.* , "Terahertz Liquid Biosensor Based on A Graphene Metasurface for Ultrasensitive Detection with A Quasi-Bound State in the Continuum," *Advanced Materials* , vol. 36, no. 11, Nov. 2023, doi: 10.1002/adma.202310493 .

[19] O. A. M. Abdelraouf *et al.* , "Recent Advances in Tunable Metasurfaces: Materials, Design, and Applications," *ACS Nano* , vol. 16, no. 9, pp. 13339–13369, Aug. 2022, doi: 10.1021/acsnano.2c04628 .

[20] J. Wang, J. Kühne, T. D. Karamanos, C. Rockstuhl, S. A. Maier, and A. Tittl, "All-Dielectric Crescent Metasurface Sensor Driven by Bound States in the Continuum," *Advanced Functional Materials* , vol. 31, no. 46, Aug. 2021, doi: 10.1002/adfm.202104652 .

[21] L. Huang, L. Xu, D. A. Powell, W. J. Padilla, and A. E. Miroshnichenko, "Resonant leaky modes in all-dielectric metasystems: Fundamentals and applications," *Physics Reports* , vol. 1008, pp. 1–66, Jan. 2023, doi: 10.1016/j.physrep.2023.01.001 .

[22] Z. Ren, Z. Zhang, J. Wei, B. Dong, and C. Lee, "Wavelength-multiplexed hook nanoantennas for machine learning enabled mid-infrared spectroscopy," *Nature Communications* , vol. 13, no. 1, p. 3859, Jul. 2022, doi: 10.1038/s41467-022-31520-z .

[23] P. T. Probst *et al.* , "Mechano-tunable chiral metasurfaces via colloidal assembly," *Nature Materials* , vol. 20, no. 7, pp. 1024–1028, Apr. 2021, doi: 10.1038/s41563-021-00991-8 .

[24] T. C. Tan *et al.* , "Active Control of Nanodielectric-Induced THz Quasi-BIC in Flexible Metasurfaces: A Platform for Modulation and Sensing," *Advanced Materials* , vol. 33, no. 27, May 2021, doi: 10.1002/adma.202100836 .

[25] Y. Zhang *et al.* , "Electrically reconfigurable non-volatile metasurface using low-loss optical phase-change material," *arXiv (Cornell University)* , vol. 16, no. 6, pp. 661–666, Apr. 2021, doi: 10.1038/s41565-021-00881-9 .

[26] F. J. García-Vidal *et al.* , "Spoof surface plasmon photonics," *Reviews of Modern Physics* , vol. 94, no. 2, May 2022, doi: 10.1103/revmodphys.94.025004 .

[27] F. Richter *et al.* , "Gradient High-Q Dielectric Metasurfaces for Broadband Sensing and Control of Vibrational Light-Matter Coupling," *Advanced Materials* , vol. 36, no. 25, Mar. 2024, doi: 10.1002/adma.202314279 .

[28] L. Kühner *et al.* , "Unlocking the out-of-plane dimension for photonic bound states in the continuum to achieve maximum optical chirality," *Light Science & Applications* , vol. 12, no. 1, p. 250, Oct. 2023, doi: 10.1038/s41377-023-01295-z .

[29] A. John-Herpin, D. Kavungal, L. von Mücke, and H. Altug, "Infrared Metasurface Augmented by Deep Learning for Monitoring Dynamics between All Major Classes of Biomolecules," *Advanced Materials* , vol. 33, no. 14, Feb. 2021, doi: 10.1002/adma.202006054 .

[30] D. Conteduca, I. Barth, G. Pitruzzello, C. Reardon, E. R. Martins, and T. F. Krauss, "Dielectric nanohole array metasurface for high-resolution near-field sensing and imaging," *Nature Communications* , vol. 12, no. 1, p. 3293, Jun. 2021, doi: 10.1038/s41467-021-23357-9 .

[31] S. S. Olyaee, M. Najafgholinezhad, and H. Alipour Banaei, "Four-channel label-free photonic crystal biosensor using nanocavity resonators," *Photonic Sensors*, vol. 3, no. 3, pp. 231–236, 2013.

[32] R. Singh, W. Cao, I. Al-Naib, L. Cong, W. Withayachumnankul, and W. Zhang, "Ultrasensitive terahertz sensing with high-Q Fano resonances in metasurfaces," *Applied Physics Letters*, vol. 105, no. 17, 2014.

[33] S. Wan, S. Yuan, K. Dai, Y. Song, and F. Zhou, "Electromagnetically induced transparency in a planar complementary metamaterial and its sensing performance," *Optik*, vol. 126, no. 5, pp. 541–544, 2015.

[34] S. Sahu, J. Ali, P. P. Yupapin, and G. Singh, "Porous silicon based Bragg-grating resonator for refractive index biosensor," *Photonic Sensors*, vol. 8, pp. 248–254, 2018.

[35] G. An, S. Li, T. Cheng, X. Yan, X. Zhang, X. Zhou, and Z. Yuan, "Ultra-stable D-shaped optical fiber refractive index sensor with graphene-gold deposited platform," *Plasmonics*, vol. 14, pp. 155–163, 2019.

[36] Z. Wang, Z. Geng, and W. Fang, "Exploring performance of THz metamaterial biosensor based on flexible thin-film," *Optics Express*, vol. 28, no. 18, p. 26370, 2020.

[37] S. K. Patel, J. Parmar, H. Trivedi, R. Zakaria, T. K. Nguyen, and V. Dhasarathan, "Highly sensitive graphene-based refractive index biosensor using gold metasurface array," *IEEE Photonics Technology Letters*, vol. 32, no. 12, pp. 681–684, 2020.

[38] J. Surve, S. K. Patel, and J. Parmar, "Design of cost-efficient graphene metasurface-based pregnancy test with NOR gate realization and parametric optimization," *IEEE Sensors Journal*, vol. 22, no. 24, pp. 23937–23944, 2022.